

RSC Advances



This is an *Accepted Manuscript*, which has been through the Royal Society of Chemistry peer review process and has been accepted for publication.

Accepted Manuscripts are published online shortly after acceptance, before technical editing, formatting and proof reading. Using this free service, authors can make their results available to the community, in citable form, before we publish the edited article. This *Accepted Manuscript* will be replaced by the edited, formatted and paginated article as soon as this is available.

You can find more information about *Accepted Manuscripts* in the [Information for Authors](#).

Please note that technical editing may introduce minor changes to the text and/or graphics, which may alter content. The journal's standard [Terms & Conditions](#) and the [Ethical guidelines](#) still apply. In no event shall the Royal Society of Chemistry be held responsible for any errors or omissions in this *Accepted Manuscript* or any consequences arising from the use of any information it contains.

Physicochemical and micromechanical investigation of nanocopper impregnated fibre reinforced nanocomposite

Md. Najmul Kabir Chowdhury^{a,*}, Ahmad Fauzi Ismail^{a,*}, Maksudur Rahman Khan^b, Mohammad Dalour Hossen Beg^{b,*}, Mohd Hafiz Dzarfan Othman^a, Rasoul Jamshidi Gohari^{a,c} and Ali Moslehyani^{a,d}

^a*Advanced Membrane Technology Research Center, University Technology Malaysia, 81310 Johor Bahru, Johor, Malaysia*

^b*Faculty of Chemical & Natural Resources Engineering, University Malaysia Pahang, 26300 Gambang, Kuantan, Malaysia*

^c*Department of Chemical Engineering, Islamic Azad University, Bardsir Branch, Bardsir, Iran*

^d*Department of Chemical and Biological Engineering, University of Ottawa, 161 Louis Pasteur St., Ottawa, ON K1N 6N5, Canada*

ABSTRACT

This paper outlines the synthesis of novel sustainable nanocomposite and its investigation of physico-chemical and mechanical properties with micromechanical models. As a novel approach, the palm oil fibres are treated with freshly prepared nano copper sols to make them strong and sustainable. Nano copper particles impregnated strong and durable fibres have been used to develop the fibre reinforced unsaturated polyester resin nanocomposite. The composite behavior has been investigated systematically by using Fourier transform infrared spectroscopy, x-ray diffraction, scanning electron microscope, thermogravimetric analysis, differential scanning calorimetry, etc. Among the composites, the nano copper particles impregnated strong

*Corresponding authors Email address: chowdhurnajmul76@yahoo.com, fauzi.ismail@gmail.com, dhbeg@yahoo.com (Mohammad Dalour Hossen Beg); Telephone: +609-549 2816; Fax: +609-549 2889.

and durable fibre (30%) reinforced unsaturated polyester resin composite has been demonstrated the highest mechanical strength. The change of weight gain is followed a typical Fickian diffusion behavior. To predict the strength of nanocomposite standard micromechanical models are analyzed and the trends are seen as mixed success. The observed properties of the developed nanocomposites indicate that they can be considering for indoor to outdoor applications.

Keywords: Fibres; Mechanical properties; Micromechanical modelling; Nanoparticles; Sustainable nanocomposites

List of Abbreviations

(3-chloro-2-hydroxypropyl) trimethylammonium chloride	CHPTAC
Advanced Membrane Technology Research Center	AMTEC
American Society for Testing and Materials	ASTM
Attenuated total reflectance	ATR
Cationized fibre	CF
Cationized fibre reinforced composite	CF-C
Differential scanning calorimetry	DSC
Empty fruit bunch	EFB
Fourier transform infrared spectroscopy	FTIR
Full width at half maximum	FWHM
Inverse Rule of Mixture	IROM
Nano copper sol	NCuS
Nanoparticles	NPs
NCuS treated fibre	NF
NCuS treated fibre reinforced composite	NF-C
Palm oil fibre	POF
Palm oil fibres	POFs

Poly (vinyl alcohol)	PVA
Rule of Mixture	ROM
Scanning electron microscope	SEM
Tensile modulus	TM
Tensile strength	TS
The International Organization for Standardization	ISO
Thermogravimetric analysis	TGA
Untreated fibre reinforced composite	UF-C
Untreated fibre	UF
Virgin resin	VR
X-ray diffraction	XRD

1 Introduction

In materials science, the recent interests of nanotechnology demand the development of novel and sustainable materials, which may have multi-functional application. This status of nanomaterials onwards the development of nanostructured polymeric material like nanoparticle impregnated natural fibre reinforced nanocomposites¹. Due to this motivation, development of sustainable nanocomposite is one of the hastily growing areas of sustainable material research². Under nanotechnology, by using a *bottom-up* approach the materials of nanocomposites may be produced, where the materials are developed from atoms, molecules, fibres, nanoscale particles modified fibres, and some other supplementary structural constituents tailored from them^{1, 3}. Almost every day, scientists and engineers are revealing the nanostructured materials application with elucidation of their properties from nanoscopic to macroscopic aspects⁴. To design a multi-functional natural fibre based nanocomposites the required vital and beneficial information is to explain how the nanoscopic material can influence the macroscopic properties of the overall structure.

To know adequately about the nanoscopic sustainable materials today, green composite research efforts are getting popular because of the need for invention of advanced materials, conservation of the environment, reduction of carbon dioxide release and plastic waste into the environment⁵. Research efforts are also uplifting for the development and application of environmentally friendly and sustainable bio-reinforced green composites for use in automotive, medical fields, construction, packaging and indoor-outdoor applications. For instance, Daimler Chrysler used the composite of flax–sisal fibre mat with an epoxy matrix as door panels of the Mercedes Benz E-class model. Coconut fibres bonded with natural rubber latex are being used in the seats of the

Mercedes Benz A-Class model⁶. Biodegradable and sustainable lignocellulosic fibres can give sound thermal and insulating performances and even they are easily recyclable also. Logically, these benefits of lignocellulosic fibres attract the automotive industry people. It has been reported⁷⁻⁹ that addition of nanoparticles to base polymers confers to improve the properties that make them usable in automotive, construction and medical areas. The properties, which have been shown to improve substantially, are mechanical properties such as strength, elastic modulus and dimensional stability.

Basically, a composite is a unification of numerous components, as a whole, which acts as a new material with the expected superior properties. The necessary condition for making a composite is the bonding between the matrix and reinforcement^{10, 11}. The site of this necessary bonding in composite is the fibre-matrix interface, and often this site is also considered as a distinct phase called the interphase. The mechanical performances of a composite material are linked to the bonding strength of fibre-matrix interface, geometry and dissemination of the reinforcement, along with the properties of the discrete phases also. To improve the mechanical strength of composites the possible two ways are: expanding the capability of material system and improving the properties of discrete phases. Consequently, it is thought that the properties of fibre reinforced composites can be further improved if the matrix is modified by the addition of NPs¹²⁻¹⁴. In the past, for the production of nanocomposites major attention had been drawn to synthetic materials such as aliphatic polyesters, aliphatic-aromatic polyesters, polyvinyl alcohols, polyester amides, polystyrene, glass and carbon fibres, nanoclays, and carbon nanotubes etc. However, the usage of such synthetic material are involved with great question¹⁵ as denying of organic waste deposition and their pollution. Conversely, natural polymers (like POFs), naturally own some favorable properties which are manifold forwarded them to use as a reinforcing agent

compare with the synthetic polymers. The notable benefits of natural fibres are available, biodegradable, renewable, cheap, etc. These advantages of the natural polysaccharides facilitate the material chemists to find out the scope of them to exploit the possibility for the preparation of new and sustainable materials¹⁶.

However, sometimes natural fibres are inappropriate for desired usages owing to their below standard performances. These properties of fibre-reinforced composites can be further improved if the matrix is modified by the NPs or by the loading of NPs impregnated fibres. Due to the nanometer size characteristic of NPs, nanocomposites also possess superior property than the conventional composites, and maximizing the required material properties can show this superiority. Therefore, the goal of this research is to develop a new type of sustainable nanocomposite, including the preparation and characterization of NCuS treated POF reinforced hybrid composites. With this aim, NCuS impregnated strong and durable POFs have been processed as a reinforcing agent of the nanocomposites. This new reinforcing agent has been introduced with unsaturated polyester resin to develop the novel nanocomposite material. The possibility of use as reinforcing agent for composites of POFs, which are waste products of palm oil mills, has been addressed in this article. Moreover, the way of obtaining new nanocomposite is also noteworthy. The properties of the prepared nanocomposite materials have been investigated by helping the Morphological (SEM), Chemical (FTIR, XRD, TGA and DSC) and Physico-Mechanical (mechanical and absorption) techniques. The mechanical performances have been analyzed by elaborating the tensile, flexural and impact properties, and water absorption kinetics are also reported here. Moreover, some micromechanical models such as Rule of Mixture, Inverse Rule of Mixture and Halpin-Tsai have also been analyzed to present a complete material property about the developed nanocomposites.

2 Materials and Method

Copper (II) chloride dihydrate salt ($\text{CuCl}_2 \cdot 2\text{H}_2\text{O}$) of 98% purity and analytical grade sodium hydroxide were procured from Merck, Germany. Fully hydrolyzed PVA of molecular weights $M_w = 70000$, sodium borohydride (NaBH_4) Reagent Plus (purity 99%), ascorbic acid (purity 99.7%) and 60% solution of CHPTAC solution were purchased from Sigma-Aldrich. 2-butanone peroxide (Laboratory grade) taken as a cross-linker or hardener. Laboratory grade sodium hydroxide and acetone (Merck, Germany), were used and procured through Permula Chemicals Sdn Bhd., Malaysia. Raw EFB fibres were collected from the LKPP Corporation Sdn. Bhd., Kuantan, Malaysia. The untreated POF was of golden-brown color with an average diameter of 0.19 mm. Unsaturated polyester resin or virgin resin (code: 268BQT) was chosen as composite matrix, which was procured from local market through PERMULA Chemicals Sdn Bhd Malaysia.

The synthesis of $\text{NCuS}^{14, 17}$ has been started with 0.5% (w/v) PVA solution in DI water. Thereafter, 100 mg $\text{CuCl}_2 \cdot 2\text{H}_2\text{O}$ and 5.0 g ascorbic acid were added subsequently in 100 mL PVA solution with adequate stirring. To get the Cu NPs, required amount of 0.347 M, NaBH_4 solution was added drop-wise in the previously found reaction mixture and the ultimate mixture was conducted for continuous stirring up to 2 hours. The morphology of NPs (as shown in Figure 1) clarify that the particles developed in the sol are in sizes in the order of a few nanometers with spherical shape. The average particle size of NPs in this sol is about 2.5 nm.^{14, 17}

2.1. Preparation of composites

First of all, NCuS has been synthesized and the route is followed from our own work and its characterization was also done previously^{14, 17}. After that, impregnation of NCuS in

cationized fibres has been done. To do that the cationization of fibres as well as the NCuS impregnation protocol was adopted from the previously done own work^{14, 17} and the details of this modification and characterizations were discussed there.

To develop the composites, the UFs were chopped first where the length was ~3 mm. Thereafter, the UFs were treated with CHPTAC solution and then followed by NCuS treatment. During composite making, such types of treated and untreated fibres of different percentages (0, 10, 20, 30 and 40% (v/v)) were used. Initially, virgin resin was mixed with 1 wt. % of 2-butanone peroxide (curing agent) for the matrix preparation of the composite. Then required amount of chopped POF was mixed with the resin solution. The POF–VR composites were prepared by hand mixing technique with the help of the mold made from aluminum plate. This technique was continued until the proper mixing of the resin with the fibre was completed. Thereafter, the mixture was left to cure for 24 h at room temperature¹⁸. In the case of composites, the volume fraction of fibre (V_f) was calculated as per the following formula (Eq. 1):

$$V_f = \frac{\frac{w_f}{\rho_f}}{\frac{w_f}{\rho_f} + \frac{w_m}{\rho_m}} \quad (1)$$

Where, W_f and W_m are the weight of fibre and matrix respectively, ρ_f and ρ_m are the density of fibre and matrix respectively.

2.2 Characterization Techniques

2.2.1. Fourier transformed infrared spectroscopy

The FTIR spectra of different fibres and their composites have been reported here by showing the graphs of absorption frequency versus transmittance (%). The peaks have been recorded over the frequency range 4000–650 cm^{-1} using a Thermo Scientific Model Smart

Performer ATR accessory of Ge crystal, attached to a Thermo Scientific spectrophotometer (Model Nicolet Avatar-370) with a single bounce. The signals have been recorded by following the parameters: angle of incidence 45°, sampling area 2 mm; number of background scans, 32; number of scans, 32; optical resolution, 4.00 cm⁻¹. The degree of cationization (*C*) has been calculated from the spectrum with the help of the following relation (Eq. (2)):

$$C = \left(\frac{I_{1648} - I_{1495}}{I_{1648}} \right) \times 100\% \quad (2)$$

Where, I_{1648} and I_{1495} are the maximum intensities of peak at 1648 and 1495 cm⁻¹, respectively.

2.2.2. Scanning electron microscopy

Treated and untreated POF reinforced nanocomposites surfaces were investigated by using a scanning electron microscope. In this purpose a tabletop scanning electron microscope (Model: TM 3000, Hitachi) was used. Samples were mounted on specimen holders with carbon tape and sputtered by platinum to make them conductive prior to SEM observation.

2.2.3. Mechanical properties of composites

A Shimadzu (Model: AG-1) Universal tensile testing machine was used to perform tensile tests in accordance with ASTM D638-77a standards. The displacement was measured with a 50 mm extensometer. The specimens were tested at a rate of 5 mm per minute. The elastic modulus, failure strain and tensile strength were calculated from the stress–strain curve. Flexural tests were performed on the same machine using the 3-point bending method as per ASTM D790-71 standard. A Ray-Ran Universal Pendulum Charpy Impact System carried out the impact testing according to the EN ISO 179. The adopted test method was consistent with ASTM D256-78 method B. The impact velocity was 2.9 m/s with hammer weight of 0.475 kg. All the test specimens were un-notched. A total of ten samples was tested and the mean value of the

absorbed energy taken. The impact strength (kJ/m^2) was calculated by dividing the recorded absorbed impact energy with the cross-sectional area of the specimens.

2.2.4. Thermogravimetric analysis of composites

Thermal measurements of the composite samples were performed to study the thermal stability characteristics of the composites by a TGA (Q500 V6.4, Germany) in a platinum crucible under nitrogen atmosphere (flow rate 40–60 mL/min) with a heating rate of 20 °C /min in the temperature range of 30–600 °C.

2.2.5. Differential scanning calorimetric analysis of composites

The crystallization behaviour of different fibre reinforced composite was measured using a differential scanning calorimeter, (Q500, V6.4, and Germany). Samples (~5 mg) were taken and placed in aluminum capsules, and then heated from 40 to 350 °C at the rate of 20 °C /min to eliminate the heat history before cooling at 20 °C /min.

2.2.6. X-ray diffraction analysis

X-ray diffraction patterns of the resin and composites were studied by using a Rigaku MiniFlex II (30 kV and 15 mA), Japan, equipped with computer-controlled software to set up the apparatus and analyze the data. The disc specimens were prepared for each category of composites by maintaining the same thickness. To prepare the disc specimen 1.0 g of the composite sample was compressed in a cylindrical mold with a pressure of 1 MPa. During the data recording the specimens were scanned step-wise. The parameters of scanning have been followed: in the range of scattering angle (2θ) between from 3° to 80° at the rate of 2°/minute with a step of 0.02°, using the CuK_α radiation of wavelength $\lambda = 1.541 \text{ \AA}$. The data have been

presented in terms of the diffracted X-ray intensity (I) versus 2θ . To calculate the X-ray crystallinity ($X_{x\text{-ray}}$), Segal's method and the following equation (3) has been applied¹⁹:

$$X_{x\text{-ray}} = \left(\frac{I_{002} - I_{am}}{I_{002}} \right) \times 100 \quad (3)$$

Where I_{002} is the maximum intensity of 002 reflections from the crystalline and amorphous components, and I_{am} is the minimum intensity of diffraction from the amorphous part of fibres. During the calculation process, the height of the (002) peak was used at a $2\theta \approx 22^\circ$, while the intensity of I_{am} was taken from the minimum intensity between the (002) and (110) peaks at a $2\theta \approx 16^\circ$. The average size of the cellulose crystallites, D_{hkl} , was determined with the full width at half-maximum of the (002) peak by using the following Scherer formula¹⁹:

$$D_{hkl} = \frac{0.9\lambda}{\beta \cos\theta} \quad (4)$$

Where, β is the FWHM (in radians) and θ is the diffraction angle. The β value was determined by curve fitting after subtracting the amorphous background. The Gaussian curve was fitted at the top of the peak for determining β and the position using an appropriate program.

2.2.7. Water absorption behavior of composites

To study the water absorption behaviour of the developed composites rectangular specimens were taken where the dimensions (length \times wide) are 30×28 mm. The test of water absorption was done as per standard test method ASTM D570. The initial weight (W_0) of the specimens was measured after oven drying at 50°C for 24 h. After the withdrawal of the specimens from the water bath/tank, surface water was removed with absorbing paper and then weighed (W_1) by a calibrated analytical balance. The water uptake percentage at any time (t) is represented as W_t , which is calculated by following the Eq. (5). The immersion was continued

until the saturation with water molecule. All of the used results were taken from the average value of three samples for each type of composite material.

$$W_t = \left(\frac{W_1 - W_0}{W_0} \right) \times 100 \quad (5)$$

Where, W_0 is the dry initial weight, W_1 is the weight after immersion in water.

According to the Fick's law, the concentration gradient is the driving force for the diffusion of water and the quantity of diffusion is a function of time. Usually, the prediction of Fick's law is satisfactorily valid for the water absorption behaviour. In the case of this prediction, the absorbed water mass increases linearly with the square root of time, afterwards slows down up to an equilibrium plateau. The coefficient of diffusion, D could be measured from the following relation²⁰:

$$D = \pi \left[\frac{d}{4M_m} \right]^2 \left[\frac{M_2 - M_1}{\sqrt{t_2} - \sqrt{t_1}} \right]^2 \quad (6)$$

Where, M_m is the maximum moisture content, d is the thickness of the sample, t_1 and t_2 are the selected points in the initial linear portion and M_2 and M_1 are the respective moisture content.

2.3 Theoretical perspectives of micromechanical models

To determine the elastic properties (experimentally or theoretically) of short fibre reinforced composites several mathematical models are worthwhile. An extensive model has several advantages; among them the top most important thing is the reduction of cost and time, which are related to the experimental follow-up. Moreover, mathematical model might be benefited enormously when it can propose the best recipe to design a highly expected material. A physical model sometimes can interpret the basic mechanisms of reinforcement. To explain the properties of composite, micromechanical models were used and the base factors are: properties

and arrangement of the constituents of the composite and matrix²¹. Furthermore, in some cases fibre aspect ratio and alignments are also considered. To explain the natural fibre reinforced composites here the considered models are:

1. Rule of mixtures;
2. Inverse rule of mixtures;
3. Halpin–Tsai equation

2.3.1. Rule of Mixtures Equation

The ROM is considered as the simplest available model for predicting the elastic mechanical properties of any reinforced composites. To estimate the elastic modulus (E_1 , in one-direction) of composite material, it is considered that both the fibre and matrix experience equal quantities of strain²². This strain is coming out due to the application of a uniform stress over a uniform cross-sectional area²³. For any reinforced composite, the apparent Young's modulus in one direction (suppose in fibre direction) the ROM equation will be the following type^{21, 22}:

$$E_1 = E_F V_F + E_M V_M \quad (7)$$

Where E and V are indicating the moduli and volume fractions respectively, on the other hand, F and M suffixes are representing fibre and matrix, respectively. The values of E_F are calculated by following the Eq. (3) of our own published work¹². Normally, ROM shows very convincing result for continuously aligned fibre reinforced composites where, due to the applied force the quantity of strain in the two components of the composites are almost equal.

2.3.2. Inverse Rule of Mixtures Equation

To estimate the elastic modulus (E_2 , in two-direction) of the composite material Reuss's assumed that the applied transverse stress will be equal in both directions (fibre and matrix)^{22, 23}. Thus, E_2 is determined by an IROM equation that is presented by different authors^{24, 21}:

$$E_2 = \frac{E_F E_M}{V_M E_F + V_F E_M} \quad (8)$$

Commonly, in most of the composites it is observed that the Young's modulus (in fibre direction) lay between the predicted positions of ROM and IROM.

2.3.3. Halpin–Tsai Equation

In 1969, Halpin and Tsai developed semi-empirical equations, those are very popular predicting the elastic properties of short fibre reinforced composites²⁵. To predict the tensile modulus of short fibre reinforced composites the Halpin–Tsai equation is presented in the following form²⁶:

$$E_1 = E_M \left(\frac{1 + \xi \eta V_F}{1 - \eta V_F} \right) \quad (9)$$

In Eq. (9) the parameter η is given as²⁶

$$\eta = \frac{(E_F/E_M) - 1}{(E_F/E_M) + \xi} \quad (10)$$

To fit the data obtained from Halpin–Tsai equation and experiments, ξ = shape fitting parameter in the above Eqs. (9) and (10). Under the parameter ξ , two things (packing arrangement and geometry of the reinforcing agents) are considered for presenting the significance of this parameter^{21, 23}. In the literature, numerous empirical equations on ξ are available, which is mainly functional to the particle shape and the modulus of the composite²⁶. If the target finding is the tensile modulus (in fibre direction) where the fibres shape is rectangular or circular then ξ is assumed from the following relation²⁶:

$$\xi = 2 \left(\frac{L}{T} \right) \text{ or } \xi = 2 \left(\frac{L}{D} \right) \quad (11)$$

Where L denotes the length of a fibre in the single-direction, and T or D is the thickness or diameter of the fibre in the three-direction. In the Eq. (11), the observed facts are, if $L \rightarrow \infty$ and

$\xi \rightarrow \infty$, then the Halpin–Tsai equation satisfy the ROM equation. On the contrary, if $L \rightarrow 0$, $\xi \rightarrow 0$ then the Halpin–Tsai equation satisfies to the IROM equation.

3 Results and Discussion

3.1 Development and characterization of nanocomposites

The UF and NF reinforced composites with commercially available polyester resins have been developed and their characterizations are performed, which is discussed in the following subsections:

3.3.1. FTIR study of composites

Figure 2 represents the FTIR spectra of (a) VR, (b) UF-C, and (c) NF-C. The main absorbance frequencies obtained for the VR are: (i) the peak around 3500 cm^{-1} , which may be attributed to the O–H stretching, (ii) the strong peaks at 3078 and 3025 cm^{-1} can be assigned to the C–H stretching vibrations from different aromatic nucleus, (iii) the clear peak at 2982 and 2888 cm^{-1} can be assigned for the C–H stretching vibrations of different aliphatic parts, (iv) the carbonyl (C=O) stretching (for ester linkage) prominently observed at 1730 cm^{-1} , (v) the aromatic C=C stretching vibration was assigned due to the observed frequency at 1635 cm^{-1} (vi) the C–H deformations appearing at 1430 – 1290 cm^{-1} , and (vii) the C–O stretching mode of vibration from the ester groups observed at 1260 – 1000 cm^{-1} . The FTIR spectrum of UF-C exhibits a joint consequence of both VR and UF. Moreover, as can be seen the peak pattern and positions of some groups especially, C=O and O–H stretching in the composite are found to be different from that of the VR. In the composites, the C=O peak is observed less prominently at 1711 cm^{-1} and comparing with the same peak of VR (prominently at 1730 cm^{-1}), and so 19 cm^{-1} red shift is observed. This may indicate that in the UF-C, the O–H groups (from fibres) formed

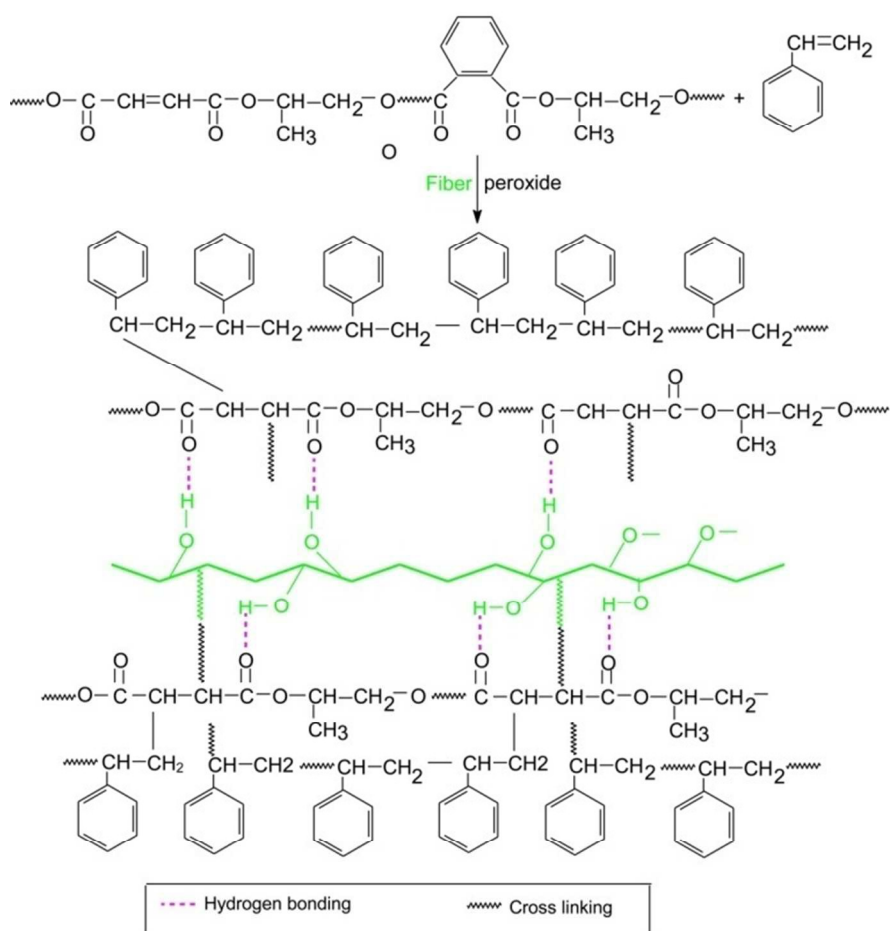
hydrogen bond with the carbonyl groups (C=O) of VR. A similar observation has also been reported for the composites by other researchers^{27,28}. Additionally, it is also mentioned that due to the usage of 2-butanone peroxide, logically some cross-linking is possible between the VR and fibres. However, the possible cross-linking centers are mainly carbon and oxygen atoms, leading to the formed bonds (due to the cross-linking) are C–C and C–O, which are also common in VR and fibres. Therefore, through FTIR the significant confirmation of cross-linking is not possible. On the other hand, the spectra of UF-C and NF-C are more or less analogous, except that the peak nature around 1684 cm^{-1} (C=O stretching), which is found due to the treatment of fibres. As in the NF-C, the assigned peak position of C=O group is at more downfield than UF-C, leading to the more redshift of C=O group takes place in NF-C and may confirming the strong interaction between C=O and O–H group.

Besides, due to the treatment of the fibre the non-cellulosic components (e.g., wax and pectin) has been removed from the fibre which facilitates the possibility of hydrogen bonding interaction between C=O and O–H group in the fibre, leading to the improvement of crystallinity of cellulose²⁸. This finding is also consistent with the XRD pattern of fibres, mechanical and water absorption properties of composites, which will also be discussed in the subsequent subsections.

The physical and chemical bonding of VR with the untreated and treated EFB fibres could be explained as follows:

Since cellulose is the main component of EFB fibres, it could be speculated that most bonding interactions occur between the O–H groups of the cellulose of EFB fibres with the C=O groups of VR. The possible sites of interaction between the cellulose of EFB fibres and VR are depicted in **Scheme 1**. Since, untreated fibres contain non-celluloses on their surfaces, it is reasonable to assume that only a limited number of O–H groups (from fibres) take part in bonding with the

C=O group of VR. Instead, the number of interact able O–H groups' increases in NF, which is due to the removal of non-celluloses from the surfaces. Thus, it is reasonable to assume that the increased exposure of the O–H groups of fibres provided improved potential for hydrogen and covalent bonding.



Scheme 1: The mechanism of interaction between resin and fibre

3.3.2. Surface morphology of POF/unsaturated polyester resin composite

The surface morphology of POF/unsaturated polyester resin composite shows the improvement of interfacial adhesion between NF and unsaturated polyester matrix can be seen from SEM micrographs of the tensile fracture surface, as shown in **Figure 3**. Comparatively weaker interfacial bonding phenomenon is observed in the case of UF-C, as shown in **Figure 3**

(a), whereas, for NF-C as shown in **Figure 3** (b), that bonding is to some degree of stronger (since the observed space between resin and fibre is ~ 4 times lower) than the UF-C. Specifically, some gaps between the fibre and matrix has been observed in both composite systems. However, this gap is ~ 4 times lower in the case of NF-C than the UF-C. In the case of NF-C, such a better interface has been observed as it contains the NF and the morphology of this fiber is significantly different than the UF. The NF fiber contains the CuNPs through the cationization (including the alkali treatment process) resulting to reduce the non-cellulosic components, which facilitate the improvement of fibre's crystallinity, along with the existing nanoparticles also provide their large surface area, to interact with the resin matrix. Furthermore, based on the properties, NPs are significantly differing from the particles of conventional size. Due to the size, aspect ratio and modifying agents NPs can improve the interfacial adhesion or bonding interaction in nanocomposites, which are reported elsewhere²⁹⁻³². The following facts are significantly noted to clarify the statement:

- (i) NPs have large aspect ratio and this large interfacial area might be suitable for an additional bonding interaction with the resin matrix²⁹. More specifically, the NPs of NFs could be involved in bonding interactions through the carbonyl (C=O) groups of matrix and the hydroxyl (-OH) groups of particle surface, as the NPs are surrounded by the PVA chain also²⁹.
- (ii) Since the interfacial interactions occur only within a very short range, the greatest interaction between modified NPs and the matrix is achieved in the case of low dose of NPs (194 mg/kg composite in this case), which can increase the interfacial area and facilitates the interfacial bonding or resin/matrix bonding³¹.
- (iii) The NF-C has better interfacial interaction than UF-C, which might be due to the NPs inter-diffusion and entanglement between the matrix/fibre at the interfacial region also³².

This finding is showing a consistency with the FTIR analysis also as in the spectrum of the NF-C showed a higher bonding interaction or more red shift of carbonyl group has been noticed.

3.3.3. *Effect of fibre loading on mechanical performances of composites*

The mechanical properties (tensile and flexural) of fibre-reinforced unsaturated polyester resin composites were investigated by varying the fibre loading, as shown in **Figure 4** and **Figure 5**, respectively. It was observed that both tensile properties increased with increasing the fibre loading, up to 30 vol.%. After that the tensile properties slightly decreased at 40 vol.% fibres loading for all types of EFB fibres. Several workers have found the same trend^{20, 33-36}. Under this finding, the general agreement is that, at high fibre loading, it is more difficult for the resin to penetrate the decreasing spaces between the fibres, leading to poor wetting, and hence, a reduction in the stress transfer efficiency across the fibre-resin interface³⁷. The treated EFB fibres such as CF and NF reinforced composites gave higher tensile properties than that of the UF reinforced composites. The results indicate that the treated fibres has the ability to make a better bonding with the resin as treatment facilitates the removal of non-cellulosic components from the fibre, enhance the surface adhesive characteristics by fibrillation process, improves the crystallinity of the fibres, and improve the fibre-matrix adhesion which is leading to higher tensile properties^{12, 13, 38}.

The flexural properties of the composites were also investigated and the results are presented in **Figure 5**. The results show the same trend as with the tensile properties obtained for the same composites. It is known that the ultimate stress of any composite depends on several factors. Among the factors, most role-playing facts are the properties of the reinforcement and matrix and the fibre volume fraction³⁹⁻⁴². The fibre mechanical properties, such as initial modulus and

ultimate tensile stress, are related not only to the chemical composition of the fibre but also in its internal structure. The observed high strength of NF-C compare with UF-C may be due to their individual fibre ultimate cellulose content and low-microfibrillar angle (i.e., the angle between the fibre axis and the fibril of the fibre)⁴¹. Furthermore, treatment can improve the fibre surface adhesive characteristics by fibrillation process²⁰. The UFs were packed together, but after the treatment fibre bundles fragmented⁴³. This phenomenon is known as fibrillation, which breaks the untreated fibre bundle down into smaller ones by removal of the non-cellulosic component like hemicellulose. It is reported that fibrillation can increase the effective surface area available for contact with the matrix, leading to the improvement of interfacial bonding⁴⁴. Therefore, for both of the studies (tensile and flexural properties), it can be concluded that the optimum fibre loading was at 30 vol.% for all of the reinforced composites and the similarity of this finding is observed elsewhere³⁶.

Apart from these, the results of flexural modulus (shown in **Figure 5** (ii)) were comparatively lower than the corresponding tensile modulus (shown in **Figure 4** (ii)). During testing the specimens experienced different kinds of stresses due to the application of two different loading conditions. In a tensile test the stresses are uniform throughout the specimen cross-section, whereas in flexure it is varied from zero in the middle to maximum at the top and bottom surfaces⁴¹. Hence, for the inhomogeneous and anisotropic material the simple tension and flexure moduli results can differ significantly. The result of flexural test is highly dependent on the properties of the materials closest to the top and bottom surfaces of the specimen, whereas a simple tension test reflects the materials average property through the thickness⁴¹. Specifically, in a flexural test the total bending deflection is the summation of a bending deflection and a shear deflection as shown in Eq. (12):

$$\delta_{flex} = \frac{Pl^3}{48EI} + \frac{Pl}{4G} \quad (12)$$

Where, δ , P , l , E , G and I are the total deflection, load within the elastic range, the span of the composite beam, modulus of elasticity, moment of inertia of the composite beam, and modulus of rigidity of the species, respectively. During the measurement of the flexural modulus, the shear contribution to the bending deflection is normally neglected⁴¹, resulting to a lower value than the tensile modulus⁴¹. NF reinforced composites showed the best flexural strength properties (60.42 MPa) compare to the UF reinforced composite (51.72 MPa). The specific flexural strength (flexural strength divided by density) of NF-C (60.42/1.123=53.76) was also higher than that for UF-C composites (51.72/1.101=46.96).

3.3.4. Charpy impact strength

Figure 6 represents the Charpy impact strength (energy absorbed/cross-sectional area) results of the virgin resin and different composites containing 30% fibre. The impact strength of different POF/unsaturated polyester resin composites is varied significantly from the virgin resin. Among them, NF reinforced composite showed maximum impact strength. The composites of UF and CF were tested and displayed low impact strengths, compared to the composite of NF (18.03 kJ/m²), which is consistent with other work, where they also reported higher impact strength of the treated fibre reinforced composites⁴⁵. Likewise, in terms of specific impact strength properties (impact strength divided by density), NF-C appears well to compare with UF-C. Among the composites, the higher impact strength of NF-C is probably due to the high strain to failure of the NF. It is well known that the impact strength of fibre reinforced composite is substantially functional to the fibre-matrix bond strength, the fibre and matrix properties^{41, 46}. In the case of fibre-reinforced composite, the possible route of impact energy dissipation

isdebonding, fibres pull out and materials (fibre or matrix) fracture. Fibre fracture dissipates less energy in comparison with fibre pull out. The former phenomenon is very common in composites with strong fibre-matrix bonding, whereas the existence of latter one is a sign of a weak bonding. Overall, it is observed that a moderate change of impact strength is observed from UF to CF composites, whereas a sharp change observed from UF to NF composites.

3.3.5 Thermal properties of composites

3.3.5.1. Thermogravimetric analysis

The thermogravimetric analysis generally involves the release of absorbed water (if any) from a sample, the “onset” of degradation of molecules in the sample, the steps of degradation and the presence of residual char in the samples²⁸. TGA plots of different EFB fibres can be seen in Figure 6. The onset of thermal degradation can be recognized by a dramatic decrease in sample weight and an increase in the temperature difference due to the exothermic combustion reactions taking place. About the TGA of fibres, it was mentioned that a sharp weight-fall occurs at elevated temperatures with a one-step thermal degradation process¹². The obvious weight-loss is found within the temperature range of 250–385 °C, which is attributed to decomposition, oxidation and burning of cellulose. It is known that the thermal stability of NF is lower than UF¹². Therefore, it is obvious to consider the composite of UF thermally more stable than the composite of NF.

Analysis of thermograms as shown in **Figure 7**, it is clear that both of the composites (UF-C and NF-C) start to lose weight at lower temperatures when compared to polyester resin. This finding indicates that due to the addition of fibre reduces the overall thermal stability of the material.

During mixing and manufacturing of composites, high shear and frictional forces are experienced by polyester resin and fibres.

During processing, it was also observed that the composites were more viscous than polyester resin due to their high fibre contents. The presence of high frictional forces between the fibres and polyester resin matrix, leading to the breakage of the polyester polymeric chains, resulting in a decrease in thermal stability of the composite⁴⁷. More specifically, from the **Figure 7** it can be seen that the thermal degradation of VR takes place mainly in one step, in which the predominating onset of weight-loss occurs at about ~ 271 °C and finishes at ~ 418 °C. On the other hand, this degradation in composites starts at a relatively lower temperature than that found in VR and also in more than one step. This may be linked with the decomposition behaviour of the components of POFs, which are present in the composites. From TGA thermograms of composites and the calculated values as presented in **Table 1**, it is clear that the weight loss began at ~ 153 °C and 125 °C for UF and NF reinforced composites respectively. However, the second onset temperatures for the same composites are 314 °C and 308 °C, respectively. This apparent downfall of thermal stability of the NF-C could be attributed to the presence of the copper nanoparticles. Since CuNP is able to show the catalytic activity and helps to conduct the heat in the composite, thus thermodynamically destabilizing its structure and reducing the thermal stability of the composite. Other authors have also reported the thermal destabilization of cellulosic fibre constituents due to the inclusion of Cu NPs⁴⁸. Moreover, the presence of higher residual char in NF-C than UF-C also agrees with the TGA thermo grams of the NF and UF. Although, degradation temperature (T_d) can be obtained from TGA investigations, it is a common practice to consider the T_d at 50% weight loss of a sample as an indicator for the

structural destabilization⁴⁹. Therefore, from TGA curves the T_d values, thus evaluated for VR, UF-C and NF-C and introduced in **Table 1**.

3.3.5.2. DSC of composites

Figure 8 depicts the DSC thermograms of VR, and the composites of UF and NF, where the fibre content is 30%. On heating, the thermo grams of composites fairly noticed only the cold crystallization exotherm (T_c) but the transitions such as a glass transition (T_g), and a melting endotherm (T_m) of all of the samples are not ascertained within this range⁵⁰. This transition temperature for all samples are disclosed in **Table 2**. Analysis observed that T_c is increasing from VR to NF-C and the trend: VR<UF-C<NF-C. This type of increasing trend of T_c in DSC thermograms of composites with treated fibre is consistent with elsewhere²⁸. These facts can be explained on the basis of the polymer chain mobility, which is easier in UF-C as compared to NF-C because the higher crystallinity of NF-C, leading to more restrictions of chain movement which is obvious and consistent with the XRD study of fibres and composites.

3.3.6. XRD Analysis

Figure 9 illustrates the XRD pattern of VR and different fibre reinforced composites. The diffraction patterns from VR can be identified by a sharp peak close to $2\theta = 20.5^\circ$. The observed peak suggests that unsaturated polyesters are poorly ordered with low degree of crystallinity. The UF shows a less diffused and intense peak at 21.1° ^{12, 14, 38}, which comes from the crystalline cellulose material of the fibres and less prominent in the composite patterns. The diffraction patterns from UF-C and CF-C are nearly similar to that of unsaturated polyester virgin resin, except the slight shifting of peak position towards the right. This result indicates that the average

molecular distance of unsaturated polyester decreases, showing a tendency to decrease the amorphousness of unsaturated polyester molecules after fibres inclusion.

On the other hand, the peak remarkably shifted to right ($2\theta = 21.6^\circ$) after inclusion of NF in VR. This fact indicates that unsaturated polyester's crystallinity in the composites increases significantly by NF reinforcement. Thus, NPs treated EFB fibres can be supposed to act as a suitable nucleating agent for crystallization of unsaturated polyester resin.

3.3.7. Water absorption of composites

Figure 10 shows the typical absorption curves for virgin polyester resin and composites, where the weight gains as a function of exposure time in water at room temperature. In each case, it is observed that at the beginning of the water absorption pattern is sharp thereafter leveled off for some range of time or it reaches equilibrium. In this study, it is thought that the change of weight gain for all samples is highly related with a typical Fickian diffusion behaviour. Comparatively, composites show higher water absorption than virgin polyester resin. However, due to the using of the treated fibre in composites the water absorption rate is decreased, it is apparent that the overall NCuS treatments of POFs reduced the water uptake of the composite system. As a chemical modification can reduce the hydroxyl group in the cell wall of the natural fibres, can fill up the void spaces of the fibres, and can increase the crystallinity and hydrophobicity of fibres, thus decreasing the water absorption of the composites¹². The result of water uptake however, is in accordance with the XRD of single fibres (presented in Chowdhury et al.,¹²) and some previous works reported by Fraga et al.⁵¹ and Vilay et al.²⁰, where they studied on jute-fibre reinforced unsaturated polyester composites.

However, for any fibrous composites, water absorption is substantially varied on fibre loading, temperature, permeability of fibre, orientation, surface protection, diffusivity, area of the exposed

surfaces, etc.⁵². Das et al.,⁵³ reported that, initially, water molecules saturate the cell wall of the EFB fibre, and then, occupies the void spaces of the fibres. **Table 2** summarizes the water absorption parameters such as diffusion coefficients (D) and the moisture content at saturation point (M_m). On the basis of D values of the composites, it is possible to say that the NF reinforced polyester composites have better resistance towards water absorption than those of UF reinforced composites. UF composite shows higher D value, which might also indicate higher void content in the UF-C system where void facilitates more pathways for water to increase the diffusion into the composites. The rate of diffusion process decreases with increasing the bonding strength or adhesion between matrix and fibres, since better adhesion indicates deficient gaps in the interracial region. According to Chowdhury et al.,¹² treatments of natural fibres can reduce the hydroxyl group in the cell wall, increase the crystallinity and hydrophobicity of the fibres, which are leading to decrease the water absorption of that fibre reinforced composites. This result is in accordance with the fibres physical properties, XRD analysis. Moreover, better adhesion between fibre and matrix can cause to the decreasing of M_m ⁵². Thus, the M_m value of NF-C is lower than that of UF-C (**Table 2**).

3.2. Theoretical modeling of composites

It is mentioned that the works on the analysis of the properties of natural fibre reinforced composites with theoretical models are very limited. Therefore, among the considered models the performance of prediction was unknown. In this article, three models were discussed using the experimental data. **Figure 11** depicts the determination of different fibre reinforced composite modulus from ROM, IROM, Halpin-Tsai model and the experimental results. In **Figure 11**, it is observed that compared with the experimental data, the predicted values obtained from ROM and IROM equations are staying in upper and lower bounds, respectively, and which

is expected also. Especially, the observed experimental data were more or less close to the IROM, which indicates that among three models IROM can predict the strength of composites with an acceptable range of success.

On the other hand, for both of the fibre reinforced composites the value of ξ (Eq. (11)), the moduli obtained from the Halpin-Tsai equation is higher than that of the experimental moduli of composites (Figure 10 (i) and Figure 10 (ii)). With the help of least square analysis using best-fit results the values of ξ were adjusted and shown in **Table 3**. From this Table, it is observed that the UF and NF reinforced composites showed 34.40 and 47.96% discrepancies respectively, which indicate that the Halpin-Tsai equation cannot perform good predictions for the moduli of both UF and NF reinforced composites. This poor prediction is happening, owing to the empirically considered geometry of UF and NF was not-fitted with the circular or rectangular cross-sections. Moreover, for NF reinforced composites showed larger discrepancies (~48%) between the calculated and best-fit values of ξ and which is believed due to the large deviation of geometry compared with the UF. This finding is supposed to the treatment changed the complex geometrical cross-sections of NF fibres, and which are not so well-fitted with the relationship of ξ shown in Eq. (11) and the conditions of the parameters²².

4. Conclusion

The notable aim of this work was to develop sustainable nanocomposite with a novel approach, especially, nanoparticle loaded natural fibre will be introduced as a reinforcing agent to make strong and durable material. The following facts are possible to summarize:

- The improvements in fibre's strength has been achieved by addition of NPs; due to the large surface area of NPs they can form inorganic network microscopically, which penetrates with polymer matrix and restricts the slips of host polymeric molecules as well as can contribute

to load sharing during stretching of the matrices, leading to the increasing of mechanical performances of polymer hosts.

- FTIR and surface morphology studies confirm the existence of better bonding interaction or adhesion in NF-C in compare with UF-C through the carbonyl and hydroxyl groups. The mechanism of interaction between fibre and resin has also been proposed.
- The mechanical properties of this NCuS impregnated POFs were made them potentially ideal reinforcing agents to enhance their mechanical property and durability of the composites. Tensile and flexural properties of the POF reinforced polyester composites were directly proportional to amount of loaded fibre. Higher mechanical (tensile and flexural) performances were obtained for treated fibre's composite compared to those of untreated fibre based composites, with a significant trend shown by NCuS treated fibre based composites. Among all of the fibre reinforced composites tested, NF reinforced unsaturated polyester resin composites (30% fibre) exhibited the highest mechanical performances. The flexural modulus was found at lower than the tensile modulus, which is believed due to the ignorance of the shear contribution to the bending deflection during the measurement of the flexural modulus.
- Higher residual char in NF-C has been explained by the existence of Cu NPs and the ultimateless-thermal stability of the NF-C has also been described with the catalytic activity of Cu NPs.
- DSC and XRD satisfy the higher crystallinity of NF-C than UF-C.
- NPs treatment decreased the water absorption of composites, and increased the tensile modulus of the composites. The change of weight gain for all samples was highly related

with a typical Fickian diffusion behavior. Lower M_m (meaning the better adhesion) has been observed for NF-C than UF-C.

- Standard micromechanical models, which are commonly used to predict the mechanical properties of traditional synthetic fibre composites, have been applied to such sustainable material system with mixed success.
- The observed findings of the nanocomposite indicate the usage in indoor to outdoor applications.

Acknowledgement

Authors are grateful to University Malaysia Pahang and University Technology Malaysia for funding this work under the grant number GRS110322. The authors thank AMTEC, University Technology Malaysia for the SEM analysis.

References

1. E. T. Thostenson, C. Li and T.-W. Chou, *Composites Science and Technology*, 2005, **65**, 491-516.
2. C. Liu, Z. Wang, Y. a. Huang, H. Xie, Z. Liu, Y. Chen, W. Lei, L. Hu, Y. Zhou and R. Cheng, *RSC Advances*, 2013, **3**, 22380-22388.
3. M. Roco, *National Science and Technology Council, The Interagency Working Group on Nanoscience, Engineering, and Technology*, Washington, DC, 1999.
4. C. Vilela, A. F. Sousa, A. C. Fonseca, A. C. Serra, J. F. Coelho, C. S. Freire and A. J. Silvestre, *Polymer Chemistry*, 2014, **5**, 3119-3141.
5. S. O. Adeosun, G. Lawal, S. A. Balogun and E. I. Akpan, *Journal of Minerals and Materials Characterization and Engineering*, 2012, **11**, 385.
6. A. B. A. Hariharan and H. A. Khalil, *Journal of Composite Materials*, 2005, **39**, 663-684.
7. J. Njuguna, K. Pielichowski and S. Desai, *Polymers for Advanced Technologies*, 2008, **19**, 947-959.
8. J. Hay and S. Shaw, *J. Mater. Res*, 2000, **7**, 962-988.
9. E. Badamshina, Y. Estrin and M. Gafurova, *Journal of Materials Chemistry A*, 2013, **1**, 6509-6529.
10. N. Azizi, E. Batebi, S. Bagherpour and H. Ghafari, *RSC Advances*, 2012, **2**, 2289-2293.
11. S. Bagherpour, *Fibre Reinforced Polyester Composites*, INTECH Open Access Publisher, 2012.
12. M. Chowdhury, M. Beg, M. R. Khan and M. Mina, *Cellulose*, 2013, **20**, 1477-1490.
13. M. Chowdhury, M. Mina, M. Beg and M. R. Khan, *Polymer bulletin*, 2013, **70**, 3103-3113.
14. M. Chowdhury, M. Beg, M. Khan, M. Mina and A. Ismail, *Colloid and Polymer Science*, 2015, **293**, 777-786.
15. K. Leja and G. Lewandowicz, *Pol J Environ Stud*, 2010, **19**, 255-266.
16. R. J. White, N. Brun, V. L. Budarin, J. H. Clark and M. M. Titirici, *ChemSusChem*, 2014, **7**, 670-689.
17. M. Chowdhury, M. Beg, M. R. Khan and M. Mina, *Materials Letters*, 2013, **98**, 26-29.
18. R. Ojah and S. Dolui, *Bioresource technology*, 2006, **97**, 1529-1535.
19. T. Inagaki, H. W. Siesler, K. Mitsui and S. Tsuchikawa, *Biomacromolecules*, 2010, **11**, 2300-2305.
20. V. Vilay, M. Mariatti, R. Mat Taib and M. Todo, *Composites science and technology*, 2008, **68**, 631-638.
21. R. M. Jones, *Mechanics of composite materials*, CRC Press, 1998.
22. A. G. Facca, M. T. Kortschot and N. Yan, *Composites Part A: Applied Science and Manufacturing*, 2006, **37**, 1660-1671.
23. C. L. Tucker III and E. Liang, *Composites science and technology*, 1999, **59**, 655-671.
24. R. M. Christensen, *Mechanics of composite materials*, Courier Dover Publications, 2012.
25. J. C. Halpin, *Effects of Environmental Factors on Composite Materials*, DTIC Document, 1969.
26. J. Affdl and J. Kardos, *Polymer Engineering & Science*, 1976, **16**, 344-352.
27. M. Chowdhury, M. Khan, M. Mina, M. Beg, M. R. Khan and A. Alam, *Radiation Physics and Chemistry*, 2012, **81**, 1606-1611.

28. A. Moshiul Alam, M. Beg, D. Reddy Prasad, M. Khan and M. Mina, *Composites Part A: Applied Science and Manufacturing*, 2012, **43**, 1921-1929.
29. S. Pradhan, F. Costa, U. Wagenknecht, D. Jehnichen, A. Bhowmick and G. Heinrich, *European Polymer Journal*, 2008, **44**, 3122-3132.
30. C. L. Wu, M. Q. Zhang, M. Z. Rong and K. Friedrich, *Composites science and technology*, 2005, **65**, 635-645.
31. M. Z. Rong, M. Q. Zhang, S. L. Pan, B. Lehmann and K. Friedrich, *Polymer International*, 2004, **53**, 176-183.
32. M. Z. Rong, M. Q. Zhang, Y. X. Zheng, H. M. Zeng, R. Walter and K. Friedrich, *Polymer*, 2001, **42**, 167-183.
33. H. Ku, H. Wang, N. Pattarachaiyakooop and M. Trada, *Composites Part B: Engineering*, 2011, **42**, 856-873.
34. M. Jacob, S. Thomas and K. Varughese, *Composites science and technology*, 2004, **64**, 955-965.
35. M. J. John and S. Thomas, *Carbohydrate polymers*, 2008, **71**, 343-364.
36. P. Sreekumar, K. Joseph, G. Unnikrishnan and S. Thomas, *Composites science and technology*, 2007, **67**, 453-461.
37. S. Sangthong, T. Pongprayoon and N. Yanumet, *Composites Part A: Applied Science and Manufacturing*, 2009, **40**, 687-694.
38. M. Chowdhury, M. Beg, M. Khan, M. Mina and A. Ismail, *Colloid and Polymer Science*, 2014, 1-10.
39. A. Peled, Workshop on high performance fiber reinforced cement composites (RILEM) HPRFCC-5, Mainz, Germany, 2007.
40. A. A. Abdulmajeed, T. O. Närhi, P. K. Vallittu and L. V. Lassila, *Dental Materials*, 2011, **27**, 313-321.
41. P. Wambua, J. Ivens and I. Verpoest, *Composites science and technology*, 2003, **63**, 1259-1264.
42. M. Baiardo, E. Zini and M. Scandola, *Composites Part A: Applied Science and Manufacturing*, 2004, **35**, 703-710.
43. S. Shibata, Y. Cao and I. Fukumoto, *Polymer testing*, 2005, **24**, 1005-1011.
44. Y. Cao, S. Shibata and I. Fukumoto, *Composites Part A: Applied Science and Manufacturing*, 2006, **37**, 423-429.
45. N.-J. Lee and J. Jang, *Composites science and technology*, 2000, **60**, 209-217.
46. J. Rout, M. Misra, S. Tripathy, S. Nayak and A. Mohanty, *Polymer composites*, 2001, **22**, 770-778.
47. G. Beckermann and K. L. Pickering, *Composites Part A: Applied Science and Manufacturing*, 2008, **39**, 979-988.
48. B. Jia, Y. Mei, L. Cheng, J. Zhou and L. Zhang, *ACS applied materials & interfaces*, 2012, **4**, 2897-2902.
49. R. V. Kumar, Y. Kolytipin, O. Palchik and A. Gedanken, *Journal of applied polymer science*, 2002, **86**, 160-165.
50. D. Suh, O. Park and K. Yoon, *Polymer*, 2000, **41**, 461-466.
51. A. Fraga, E. Frullloni, O. De la Osa, J. Kenny and A. Vázquez, *Polymer testing*, 2006, **25**, 181-187.
52. M. Mariatti, M. Nasir and H. Ismail, *Polymer testing*, 2001, **20**, 179-189.

53. S. Das, A. Saha, P. Choudhury, R. Basak, B. Mitra, T. Todd, S. Lang and R. Rowell, *Journal of applied polymer science*, 2000, **76**, 1652-1661.

LIST OF FIGURES AND TABLES

Figure 1: Morphology of CuNPs.

Figure 2: FTIR spectra of: (a) virgin resin, (b) UF and (c) NF reinforced composite.

Figure 3: SEM micrographs of the fractured surface of (a) UF-C and (b) NF-C.

Figure 4: Effect of fibre loading on (i) tensile strength and (ii) tensile modulus of the composites: (a) UF-C, (b) CF-C, and (c) NF-C.

Figure 5: Effect of fibre loading on (i) flexural strength and (ii) flexural modulus of: (a) UF-C, (b) CF-C, and (c) NF-C.

Figure 6: Charpy impact strengths of virgin resin and different fibre (30% loading) reinforced polyester resin composites.

Figure 7: TGA curves for: (a) VR, (b) UF-C and (c) NF-C.

Figure 8: DTA curves: (a) virgin resin (VR), (b) UF-C, and (c) NF-C.

Figure 9: XRD pattern of: (a) VR, (b) UF-C, (c) CF-C, and (d) NF-C.

Figure 10: Water absorption performances of virgin polyester resin: (a) untreated (b) and treated (c) fibre-reinforced composites.

Figure 11: Determination of composites' modulus containing (i) UF and (ii) NF: where, (a) experimental data, (b) ROM, (c) IROM, and (d) Halpin-Tsai.

Table 1: Thermogravimetric parameters of virgin resin and the composites

Table 2: The parameters of DSC analysis and water absorption studies for virgin resin and composites

Table 3: Calculated and best-fit values of ξ .

Table 1: Thermogravimetric parameters of virgin resin and the composites

	T_d (°C)	1 st Onset (°C)	2 nd Onset (°C)	3 rd Onset (°C)	Moisture %	Residue (%) at 595.65 °C
VR	381.86	200	334	415.5	0.83	4.52
UF-C	357.60	153	314	402.5	1.37	3.75
NF-C	355.37	125	310	400.6	2.02	5.29

Table 2: The parameters of DSC analysis and water absorption studies for virgin resin and composites

Materials	T_c (°C)	D ($\times 10^{-11}$) $m^2 s^{-1}$	M_m (%) at 360 h
VR	50.67	1.34	3.84
UF-C	103.74	120.48	9.48
NF-C	140.78	2.19	6.57

Table 3: Calculated and best-fit values of ξ .

Fibres	ξ (calculated by Eq. (11))	Best-fit ξ	Deviations (%)
UF	35.29	23.15	34.40
NF	39.74	20.68	47.96

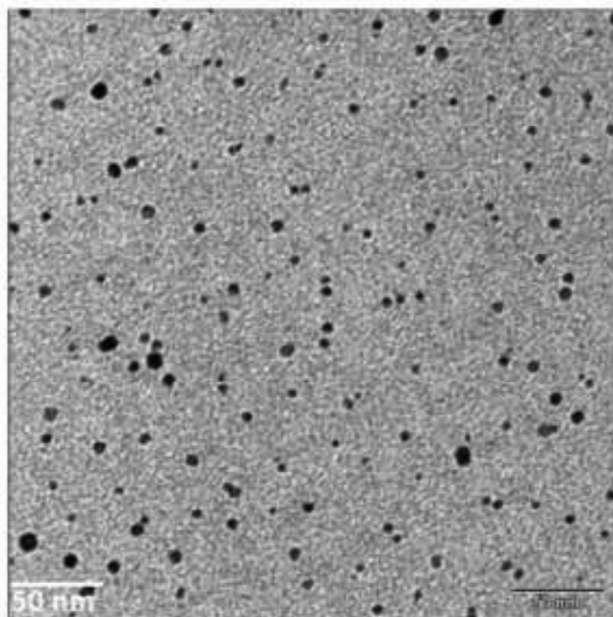


Figure 1: Morphology of CuNPs

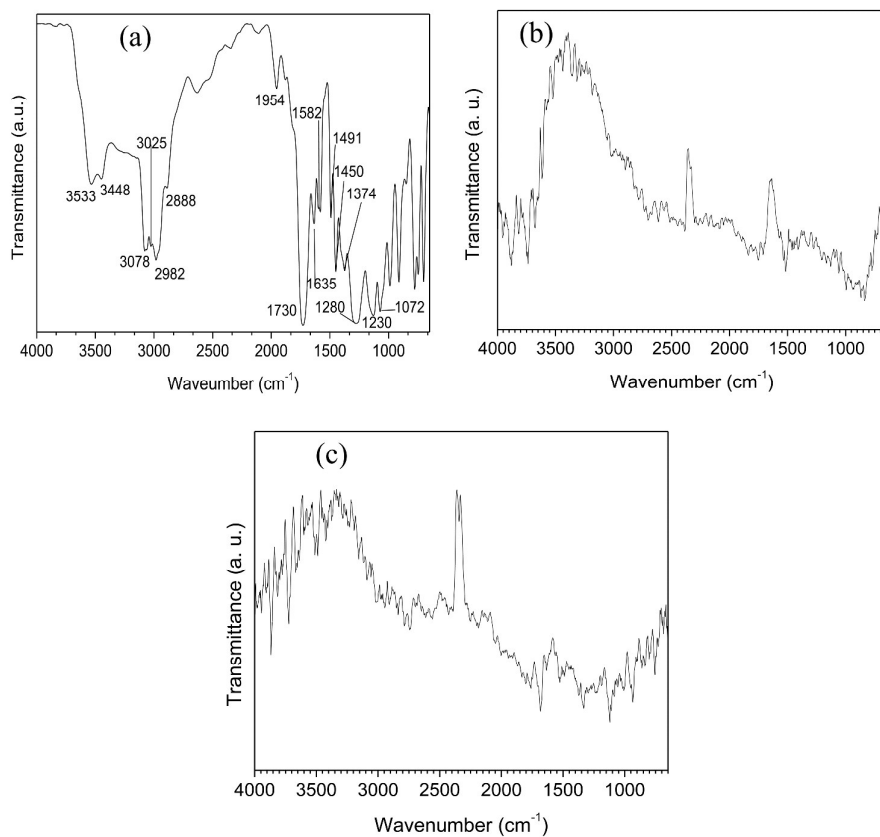


Figure 2: FTIR spectra of: (a) virgin resin, (b) UF and (c) NF reinforced composite.

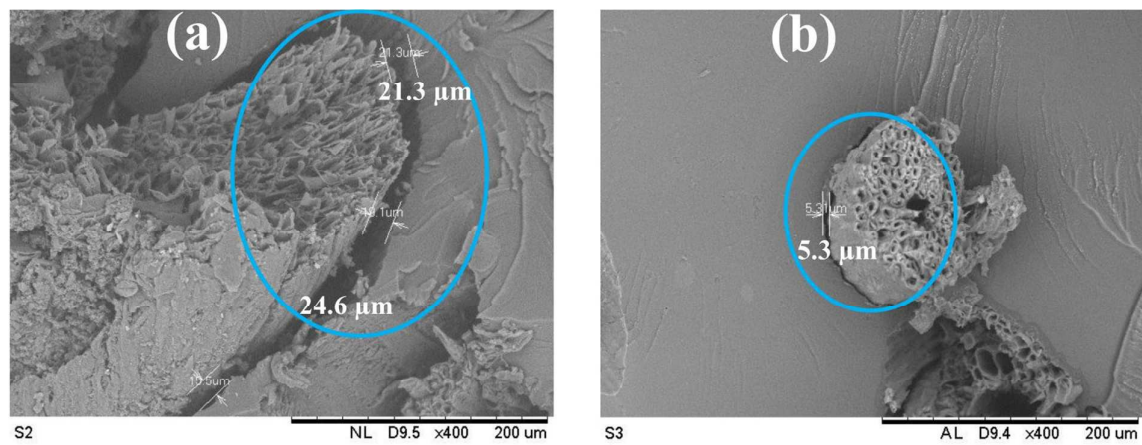


Figure 3: SEM micrographs of the fractured surface of (a) UF-C and (b) NF-C.

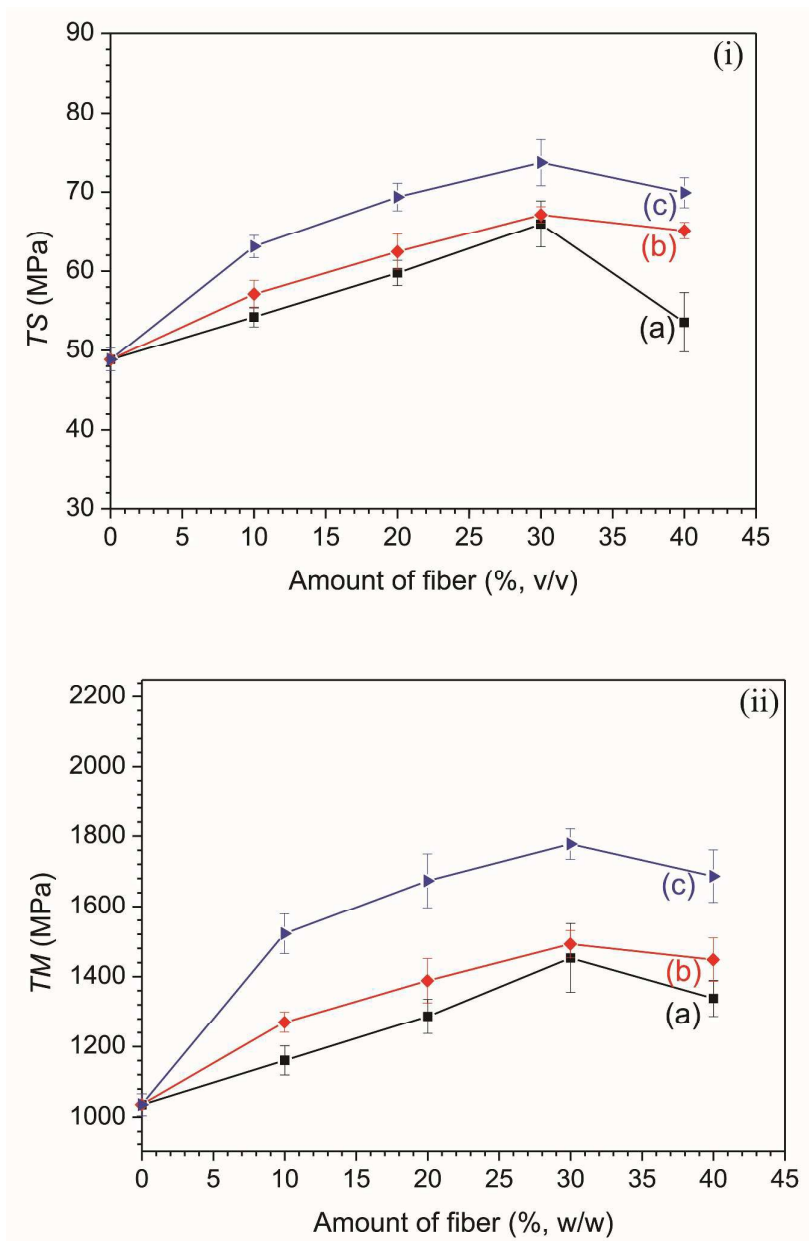


Figure 4: Effect of fibre loading on (i) tensile strength and (ii) tensile modulus of the composites: (a) UF-C, (b) CF-C, and (c) NF-C.

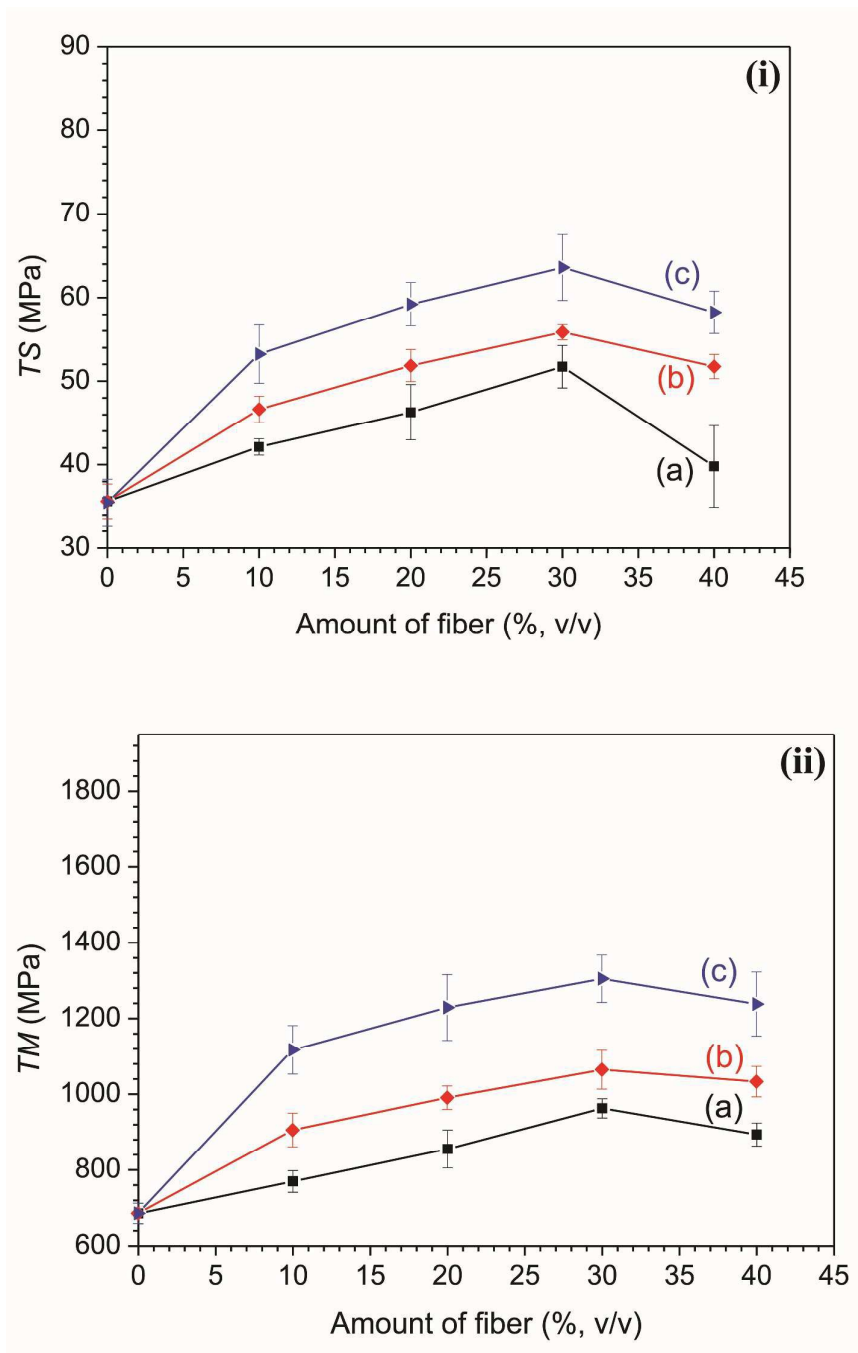


Figure 5: Effect of fibre loading on (i) flexural strength and (ii) flexural modulus of: (a) UF-C, (b) CF-C, and (c) NF-C.

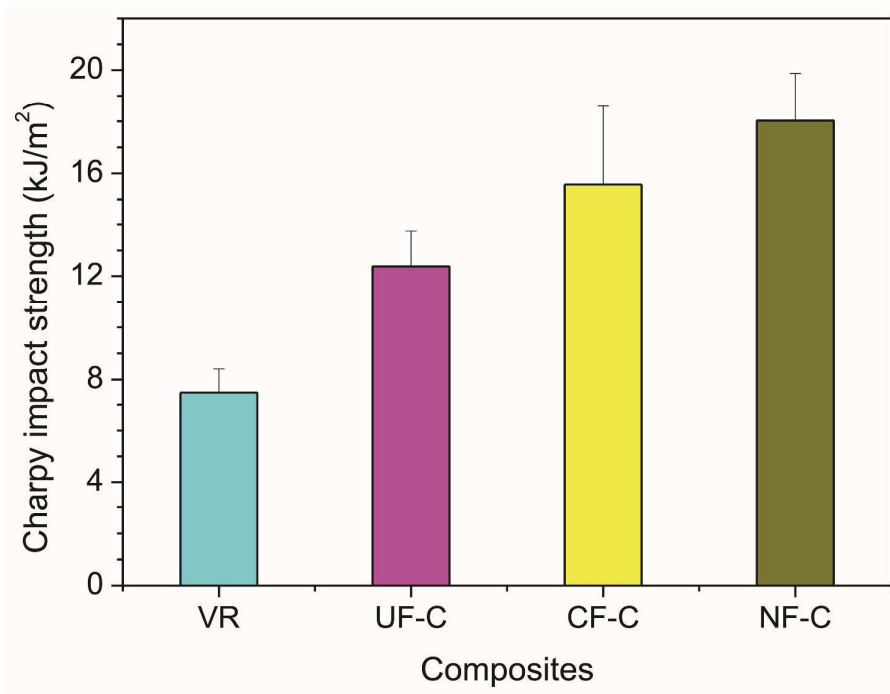


Figure 6: Charpy impact strengths of virgin resin and different fibre (30% loading) reinforced polyester resin composites.

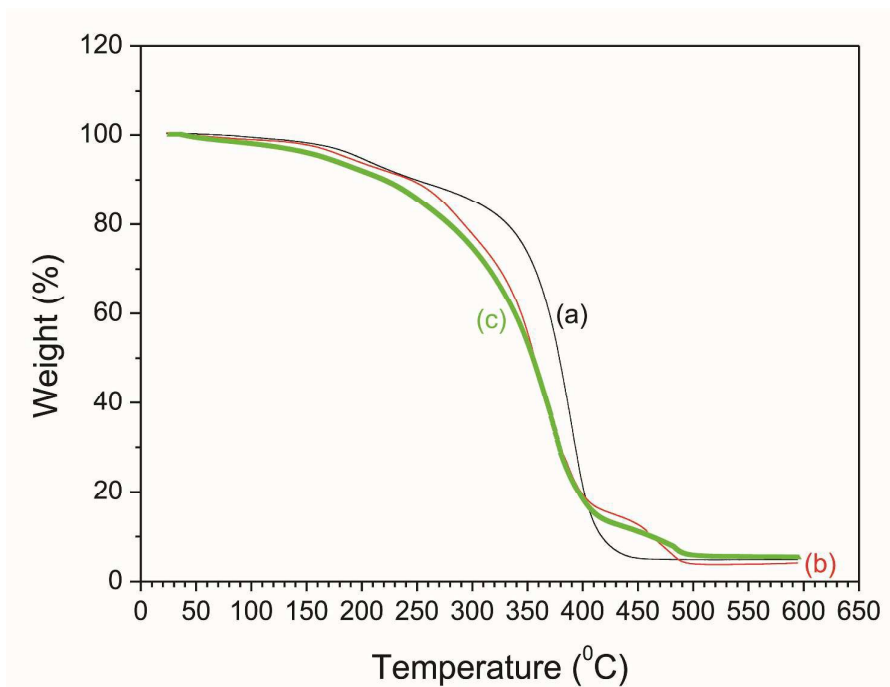


Figure 7: TGA curves for: (a) VR, (b) UF-C and (c) NF-C.

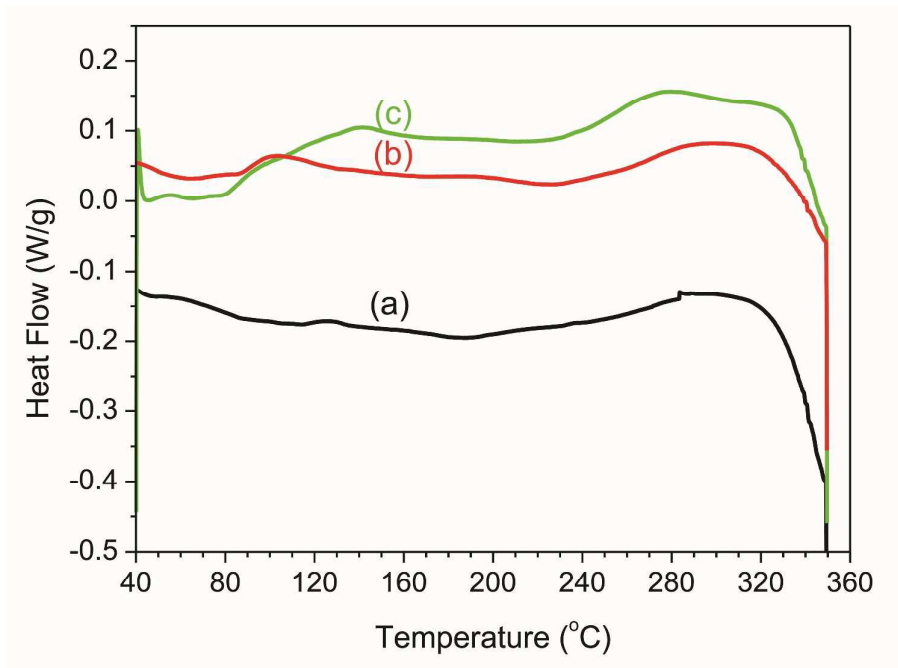


Figure 8: DTA curves: (a) virgin resin (VR), (b) UF-C, and (c) NF-C.

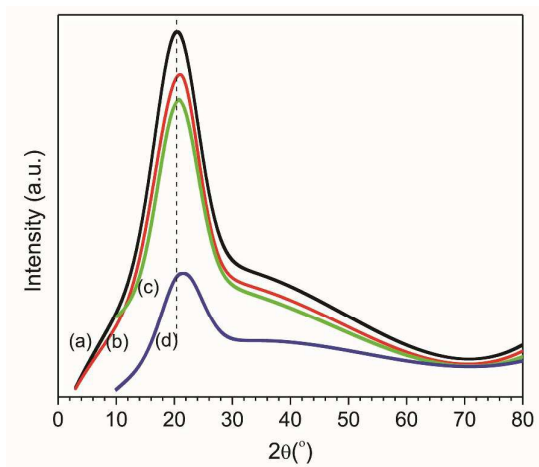


Figure 9: XRD pattern of: (a) VR, (b) UF-C, (c) CF-C, and (d) NF-C.

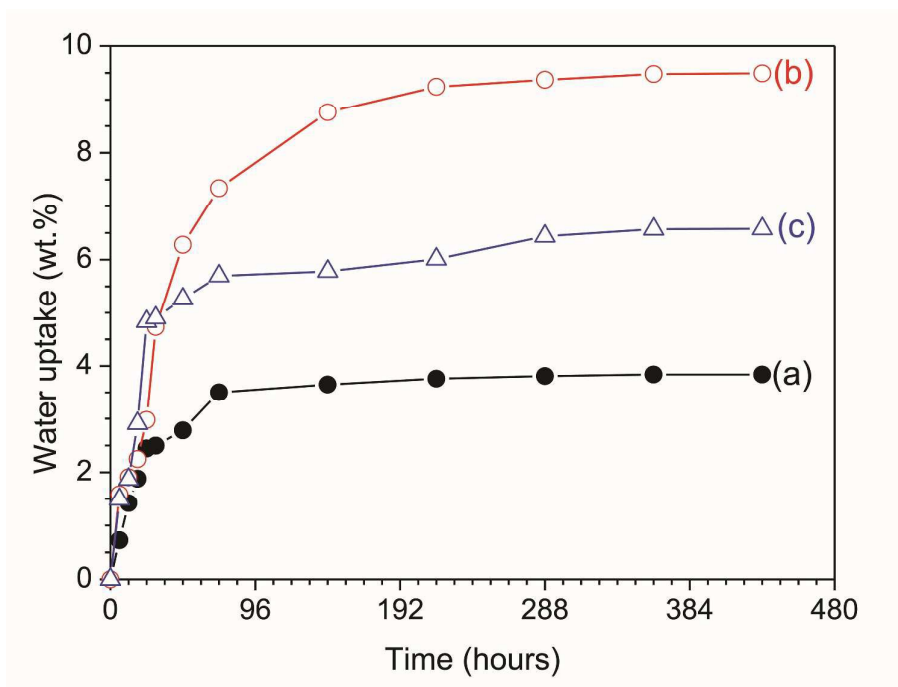


Figure 10: Water absorption performances of virgin polyester resin: (a) untreated (b) and treated (c) fibre-reinforced composites.

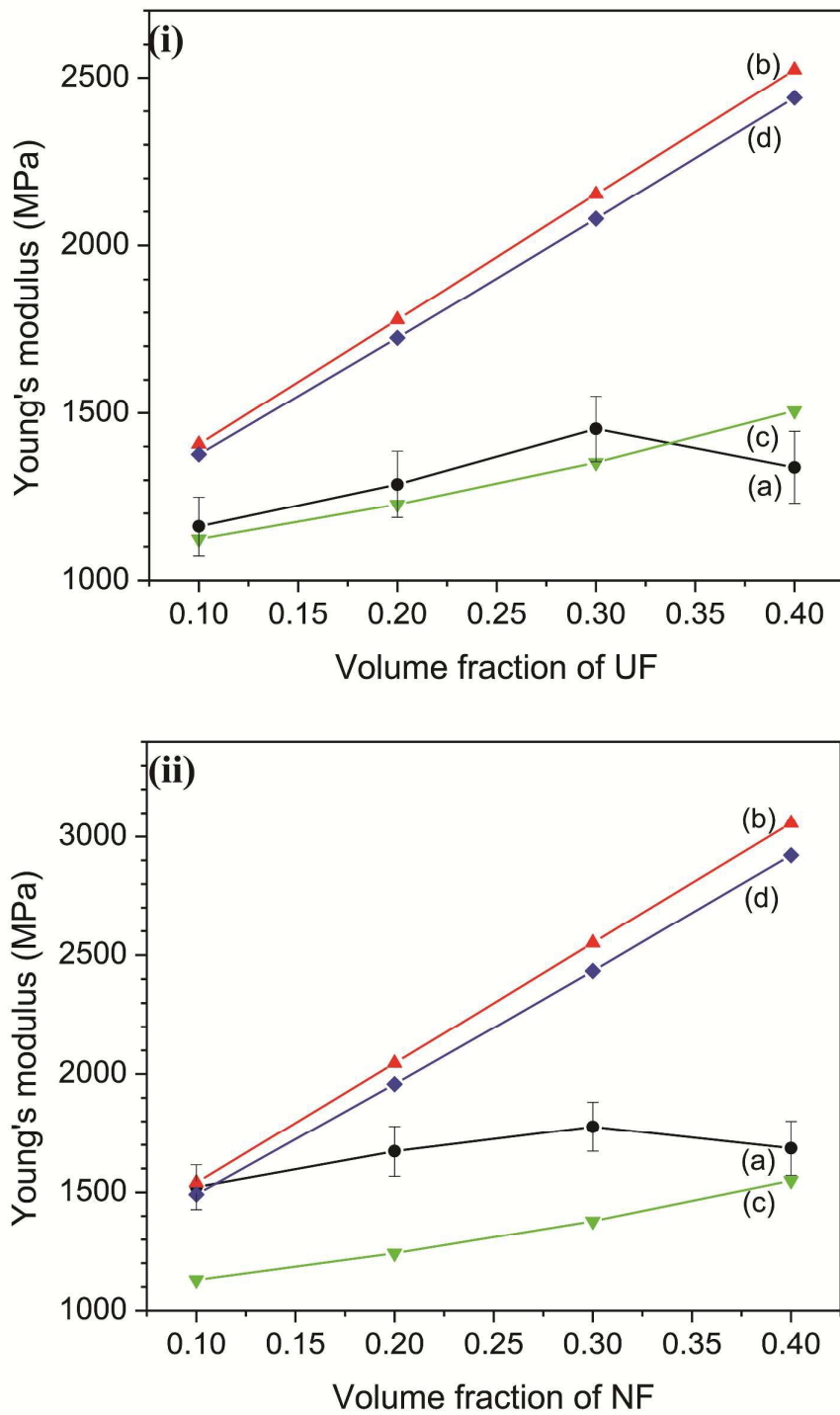


Figure 11: Determination of composites' modulus containing (i) UF and (ii) NF: where, (a) experimental data, (b) ROM, (c) IROM, and (d) Halpin-Tsai.